# Efficient Adsorption of Uranyl Ions From Aqueous Solution by Oxide Materials

**Lili Zhang**
Qinghai Normal University
**Yuantao Chen** ( chenyt@qhnu.edu.cn )
Qinghai Normal University https://orcid.org/0000-0003-0257-1352
**Meng Zhao**
Qinghai Normal University
**Yinghui Wang**
Qinghai Normal University

**Research Article**

**Keywords:** Gd2O3, Gd2O3-MgO, composite materials, uranyl ion.

**Posted Date:** May 4th, 2021

**DOI:** https://doi.org/10.21203/rs.3.rs-406684/v1

# Efficient adsorption of uranyl ions from aqueous solution by oxide materials

Lili Zhang, Yuantao Chen*, Meng Zhao, Yinghui Wang

College of Chemistry and Chemical Engineering, Qinghai Normal University, Xining, Qinghai 810008, China

Abstract: In this work, pure gadolinium oxide ($Gd_2O_3$) and mixed gadolinium oxide ($Gd_2O_3$) - magnesium oxide (MgO) composites were synthesized by simple hydrothermal method and calcination treatment. Two kinds of materials were used to remove uranyl ions from aqueous solution and characterized the structure and morphology by means of XRD, FT - IR, SEM, EDS and XPS. MgO was introduced into $Gd_2O_3$ material, which effectively avoided the agglomeration of $Gd_2O_3$ material and increased the adsorption capacity.The effects of different initial pH, initial uranium concentration and contact time on the adsorption performance of $UO_2^{2+}$ were investigated by static adsorption experiments. The thermodynamic fitting of Langmuir and Frenudlich equations showed that the adsorption process of the two kinds of materials were more consistent with the Langmuir equation. At 25℃, the maximum adsorption capacities of $Gd_2O_3$ and $Gd_2O_3$-MgO for $UO_2^{2+}$ were 473.43 $mg \cdot g^{-1}$ and 812.41 $mg \cdot g^{-1}$, respectively. Thermodynamic parameters (ΔG0<0, ΔS0>, and H0<0) indicated that the adsorption properties are exothermic and spontaneous. The possible adsorption mechanism is derived from XPS and FT-IR analysis, which mainly involves the complexation of -OH and U(VI) generated by the hydration on the surface of the materials.

Key Words: $Gd_2O_3$; $Gd_2O_3$-MgO; composite materials; uranyl ion.

## 1. Introduction

Uranium (U) is an important energy substance. The development of nuclear power industry lead to the increasing demand for uranium resources, many countries and governments attach importance to the development and utilization of nuclear energy(Cheng xu et al. 2019; Syrbua et al. 2019). At the same time, the waste generated from nuclear operations needs to be solved. $^{235}U$ has strong radioactivity and becomes the main radioactive pollutant in the nuclear power industry (Rajaei et al. 2021). The adsorption method has been widely used in the enrichment and extraction of heavy metals with low concentration because of its advantages such as good adsorption effect, low material cost, simple operation, low concentration of treated objects, and reusable adsorbent

Corresponding author: Yuantao Chen, E-mail: chenyt@qhnu.edu.cn, Tel:+86-0971-6303374, Fax:+86-0971-6303374

(Molavi et al. 2018; Kaura et al. 2019). The performance of the adsorbent is an important factor to determine its adsorption capacity for $UO_2^{2+}$ (Wang et al. 2020; Wang et al. 2019). Therefore, finding a suitable adsorbent to remove uranium from wastewater has become an important way of energy environmental protection and resource reuse.

Currently, studies on uranium adsorption materials include inorganic materials (Wang et al. 2020), organic materials (Peng et al. 2019; Yang et al. 2019) and composite materials (Zhao et al. 2019). Duan and his colleagues prepared a series of thin two-dimensional MOFs nanosheets MnS, in which the adsorption capacity of MnS-2 for uranyl ions reached 591.79 $mg \cdot g^{-1}$ when pH greater than 6 (Wang et al. 2015). Zhao and his partner studied a microbial graphene oxide (GO) composite material by immobilization of Lysinibacillus to adsorb uranium (VI) from aqueous solution, its maximum adsorption capacity is 149.3 $mg \cdot g^{-1}$ (Zhao et al. 2019). Luo et al. showed that the ability of the amine derivatives of UiO-66 to remove uranium was slightly greater than UiO-66 itself (UiO-66-$NH_2$ is 114.9 $mg \cdot g^{-1}$ and UiO-66 is 109.9$mg \cdot g^{-1}$) (Luo et al. 2016). Zhang et al. studied a three-dimensional water-stabilized $K^+$ exchange zeolite sulfide with an exchange capacity of 147.6 $mg \cdot g^{-1}$ for $UO_2^{2+}$ and a wide pH resistance (pH at the range of 2.75 ~ 10.87) (Zhang et al. 2019). Although these materials have a good adsorption effect on $UO_2^{2+}$, there are still encounter some disadvantages such as the process of preparation complexed, high cost, and the use of a large number of chemical reagents in the preparation process (Xie et al. 2020). Therefore, it is an important task to find uranyl ions adsorption materials with simple preparation process, low cost and environment friendly.

Metal-organic framework are porous coordination polymers with inorganic metal cations as the center and organic ligands as the linker (Yao et al. 2020). MOFs are considered as ideal adsorption materials for uranyl ions due to its has the advantages such as high stability, large specific surface area and adjustable structure,(Qiu et al. 2008). However, there are a large number of unreacted ligands in the pore structure of MOFs, filling its pores, which is not conducive to adsorption (Han et al. 2016). High temperature calcination can effectively remove the fillers in the MOFs structure, expose more active sites, which is favorable for the contact between active sites and uranyl ions and can improve the adsorption capacity for $UO_2^{2+}$ (Yan et al. 2018).Therefore, the study of metal oxides and mixed oxide materials calcined by MOFs has come into the perspective of scientists (Juibari et al. 2020; Mohamed et al. 2018). Metal oxide preparation is simple, environmental protection, low cost, good adsorption performance, the performance of the mixed oxide material is better than single component material because it is determined by the single component together (Abu-Dief A M et al. 2020). Compared with the parent compound, composite materials may have a more significant adsorption performance, better for heavy metal ions removal efficiency (Abudief I H et al. 2020).

In general, the world use $Gd_2O_3$ is the main component of doping $UO_3$ as the nuclear fuel uranium core. If Gd salt can be employed as the raw material to produce the adsorbent, it will not only save cost but also have great significance for uranium recovery and environmental protection. Rare earth gadolinium oxide as a kind of rare earth oxide matrix, has high crystal structure stability and thermal conductivity coefficient, good chemical stability and thermal stability and

favored by researchers (Muneer et al. 2015; Zhydachevskyy et al. 2018), these features make gadolinium oxide is widely used in fluorescent material (He et al. 2011), magnetic materials (Huang et al. 2008), catalytic materials (Qian et al. 2018) and sustained release technology (Jiu et al. 2015), etc. However, the adsorption properties of $Gd_2O_3$ are rarely studied, although the properties of other oxides doped with $Gd_2O_3$ have been extensively invented (Choi et al. 2020; Trejo-García et al. 2020), the preparation of $Gd_2O_3$-MgO composites and the adsorption effects of $Gd_2O_3$-MgO on uranyl ions have not been reported. Therefore, $Gd_2O_3$ and $Gd_2O_3$-MgO mixed oxide composites were used as adsorbents to study their adsorption properties for uranyl ions, and the adsorption mechanism was explained.

# 2.Materials and method

## 2.1 Materials

The reagents we used in the experiment were all analytically grade and no further treatment was done, mainly includeded Terephthalic acidc($C_8H_6O_4$), Gadolinium nitrate hexahydrate ($Gd(NO_3)_3·6H_2O$), Magnesium nitrate hexahydrate ($Mg(NO_3)_2·6H_2O$),

N, N-dimethylformamide(DMF), Methanol($CH_3OH$). The uranyl ions used in the experiment were obtained by dissolving uranyl nitrate hexahydrate ($UO_2(NO_3)_2·6H_2O$) in deionized water.

## 2.2 Adsorbent preparation

The $Gd_2O_3$-MgO were synthesized with traditional solvothermal and calcination methods by changing $Gd^{3+}/Mg^{2+}$ molar ratios to optimize the material. The specific steps as follows: First, A certain amount of $Gd(NO_3)_3·6H_2O$, $Mg(NO_3)_2·6H_2O$ and 0.8306 g terephthalic acid were dissolved in 30mL N, N-dimethylformamide and stirred magnetically for 30 min at room temperature to prepare the solution. The mixed solution were poured to the 50 mL Teflon-lined stainless steel autoclave, then put into the oven and slowly heated to 120℃and kept for 24h. After cooling to room temperature, washed with methanol and centrifuged for three times and each time took five minutes (8000rpm). Afterward, the product of drying in the vacuum drying oven at 60℃ were called as GD-BDC, Gd-Mg-BDC. Finally, Gd-BDC and Gd-Mg-BDC were calcined in Muffle furnace at 800℃ for 3 h to obtain adsorbents $Gd_2O_3$ and $Gd_2O_3$-MgO. After adsorption of U(VI),Two kinds of adsorbents were denoted as $Gd_2O_3$-U and $Gd_2O_3$-MgO-U, respectively.

## 2.3 Characterization

The materials were prepared by magnetic stirring apparatus (IKA RH BASIC KT/C), washed and separated by a high-speed centrifuge (H1850 cence), dried and calcined by vacuum drying oven and muffle oven furnace (YTH-4-10A), respectively. Temperature-controlled shaker (IKAKS 4000i) and inductively coupled plasma (ICPE-9000) were used for adsorption experiments and determination of uranyl ion concentration after adsorption, respectively. X-ray diffraction (XRD-6000) and the new generation Hitachi SU8010 field emission scanning electron microscope (FE-SEM) were used to characterize the crystal form and morphology of the materials. Fourier transform infrared spectrometer (Nicolet IS500) and X-ray photoelectron spectroscopy (XPS) were used to analyze the surface composition and chemical state of the adsorbents.

## 2.4 U(VI) adsorption experiments

The uranium solution needed in this experiment was prepared by dissolving $UO_2(NO_3)_2 \cdot 6H_2O$ in deionized water, and drop a small volumes of NaOH/$HNO_3$ to control the pH of the solution. A small quality of adsorbent was added to the uranyl solution and placed in a temperature-controlled shaker at 25°C and 180 r·min$^{-1}$ to oscillate for a certain time. After adsorption of uranyl ions, the supernatant was filtered into a 10 mL centrifuge tube with 0.45-μm polyethersulfone membrane fifilters, and quantitative analysis was carried out by ICPE-9000. The equilibrium adsorption capacity (Q, mg·g-1 ) of the adsorbent to uranyl ions can be calculated by the following formula: (1) (Zhao et al. 2019; Liu et al. 2020):

$$Q = \frac{C_0 - C_e}{m} \times V \qquad (1)$$

Herein, $C_0$ (mg·L$^{-1}$) is the initial concentration of the uranium solution required for the experiment; $C_e$ (mg·L$^{-1}$) is the equilibrium concentration of the solution after the $Gd_2O_3$ and $Gd_2O_3$-MgO adsorbed uranyl ions; V (L) is the volume of the uranyl solution; m (g) is the mass of the $Gd_2O_3$ and $Gd_2O_3$-MgO.

# 3. Results and discussion

## 3.1 Preparation and optimization of composite materials

The adsorbent was synthesized by hydrothermal method and calcination treatment with diffffferent $Gd(NO_3)_3 \cdot 6H_2O$/$Mg(NO_3)_2 \cdot 6H_2O$ molar ratios(1:0, 1:1, 1:1.5, 1:2). In order to research the adsorption properties of the composites for uranyl ions, different $Gd^{3+}$/$Mg^{2+}$ molar ratios were used to optimize $Gd_2O_3$-MgO materials. As shown in Fig. 1, the materials prepared with different $Gd^{3+}$/$Mg^{2+}$ molar ratios have different adsorption capacities for uranyl ions. When $Gd^{3+}$/$Mg^{2+}$= 1:1, the adsorption capacity reached the maximum, and decreased with the increase of $Mg^{2+}$. A small amount of $Mg(NO_3)_2 \cdot 6H_2O$ could increase the adsorption capacity of the $Gd_2O_3$-MgO, but when the amount of $Mg(NO_3)_2 \cdot 6H_2O$ was too much, the effect was opposite. Therefore, $Gd^{3+}$/$Mg^{2+}$= 1:1 was selected for the preparation of composite materials in subsequent experiments.

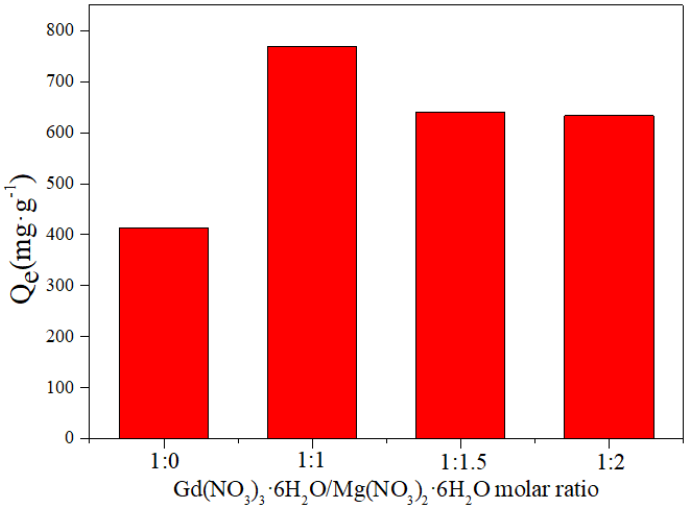

Fig. 1 Effect of $Gd(NO_3)_3·6H_2O/Mg(NO_3)_2·6H_2O$ molar ratio on $UO_2^{2+}$ adsorption.

## 3.2 Characterization of adsorbents

Fig 2(a) shows the XRD patterns of Gd-BDC ,$Gd_2O_3$, Gd-Mg-BDC and $Gd_2O_3$-MgO. The diffraction peaks of Gd-BDC and Gd-Mg-BDC are similar, and there is a characteristic peak before 10°, indicating that Gd-BDC and Gd-Mg-BDC exist in the form of MOFs rather than oxides (Fei et al. 2015). The peaks of 2θ at 20°, 28.6°, 33.1°, 47.5°, and 56.4°correspond to the (211), (222), (400), (444), and (622) planes belonged to $Gd_2O_3$ nanoparticles with cubic structure, which are consistent with the standard card of cubic phase gadolinium oxide (JCPDS 43-1014). The XRD patterns of $Gd_2O_3$-MgO not only show the diffraction peaks of $Gd_2O_3$, but also the characteristic diffraction peaks of (200), (200) and (222) of MgO at 2θ=42.9°, 62.3°and 78.6° (Wang et al. 2018), indicating the formation of $Gd_2O_3$-MgO composites. Both of the synthesized materials have sharp and strong XRD lines, which indicated the degree of crystallization is high. The structure evolvement of the synthesized $Gd_2O_3$-MgO with different moler ratios of $Gd(NO_3)_3·6H_2O/Mg(NO_3)_2·6H_2O$ were shown in Fig 2(b). It can be observed that XRD peak intensity of $Gd_2O_3$-MgO firstly increases and then decreases with the increase of the molar ratio of $Gd^{3+}/Mg^{2+}$. When $Gd^{3+}/Mg^{2+}$=1:1, the diffraction peak is the strongest, showing that the crystallinity of $Gd^{3+}/Mg^{2+}$=1:1 is the highest.

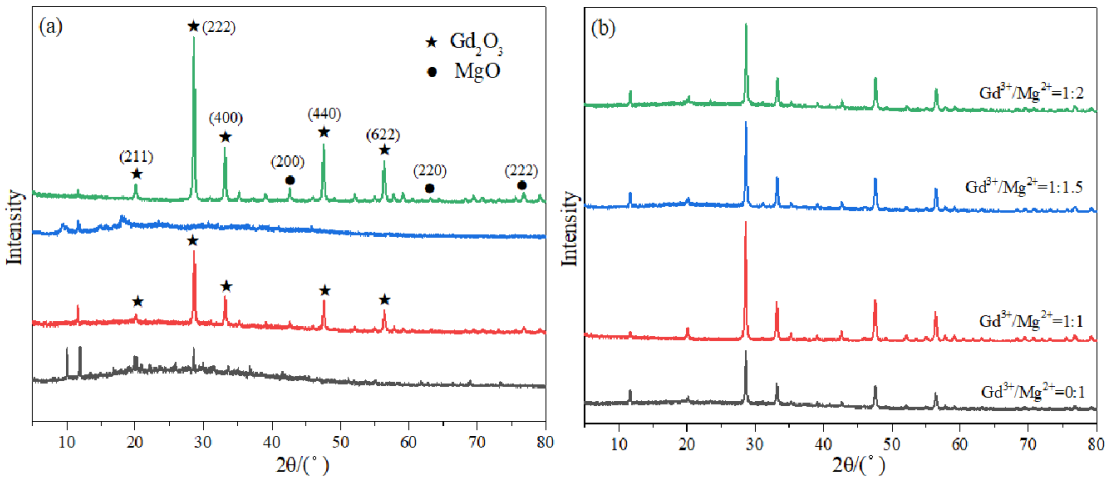


Fig 2. XRD patters (a) of two kinds of materials and their precursors and (b) of $Gd_2O_3$-MgO with different $Gd(NO_3)_3·6H_2O/Mg(NO_3)_2·6H_2O$ molar ratio.

The FT-IR spectra of fresh and used materials and their precursors were shown in Fig 3. In the spectra of $Gd_2O_3$ and $Gd_2O_3$-U (Fig 3(a)), the bonds at 547$cm^{-1}$ belongs to the Gd-O stretching vibration (Dhananjaya et al. 2014; Tamrakar et al. 2015). The uranium adsorption peak of $Gd_2O_3$-U appears at 915 $cm^{-1}$, which is caused by antisymmetric stretching vibration of O=U=O (Cheng Xu et al. 2019; Liu et al. 2016). The spectrum of the composite material is shown in Fig. 3(b), it not only shows the absorption peak as shown in Fig 3(a), but also the tensile vibration of Mg-O at 1105 $cm^{-1}$ and 1090 $cm^{-1}$ (Yunsheng et al. 2017), indicating the successful combination of MgO and $Gd_2O_3$, which is consistent with the analysis results of XRD. The absorption peaks at 1456 $cm^{-1}$ and 1620 $cm^{-1}$ were caused by the reaction of $H_2O$ and $CO_2$ on the surface of the

material to form carbonate ($CO_3^{2-}$) (Chowdhury I H et al. 2016; Chowdhury A H et al. 2015; Lin et al. 2013). The peak at 3735 $cm^{-1}$ is attributed to the free O-H vibration, which is generated by the hydration on the surface of material and suggested that the hydroxyl group is involved in the uranyl ion adsorption process (Wang et al. 2018). In the spectra of Gd-BDC and Gd-Mg-BDC, the wide band around 3400$cm^{-1}$ were due to the stretching vibration of -OH and $H_2O$ molecules on their surfaces (Wang et al. 2015); C-H stretching vibration is around 2920 $cm^{-1}$; the bond at 1683-1322 $cm^{-1}$ is the -C=C absorption peak on the benzene ring and the -C=O absorption peak in the carboxyl group attached to the benzene ring. The FT-IR spectra of the two kinds of MOFs are obviously different from the prepared nanocomposites, indicating that the metal-organic framework has been completely decomposed (Tarighi et al. 2013).

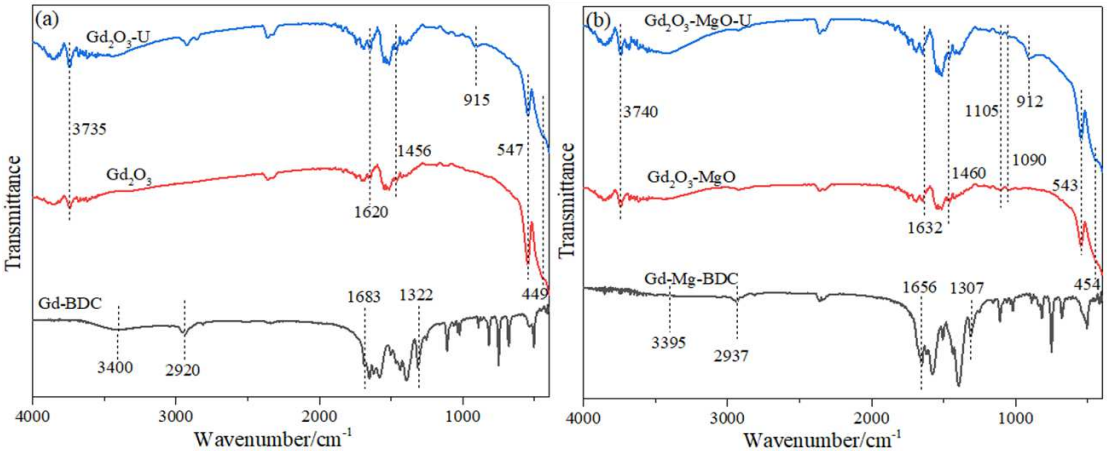


Fig 3. FT-IR spectra of $Gd_2O_3$ (a) and $Gd_2O_3$-MgO (b) before and after adsorption and their precursor.

Surface morphology analysis is shown in Fig 4. The SEM images of before adsorption: (a, b) $Gd_2O_3$, (c, d) $Gd_2O_3$-MgO. As presented from Fig (a) and (b), $Gd_2O_3$ has obvious agglomeration phenomenon, it is clear that the blade-like morphology overall. In the case of Fig (c) and (d), beyond doubt, doped with MgO has huge influence on the morphology, it is consist of spherical particles. In addition, there are a lot of pores on the surface of the $Gd_2O_3$-MgO, showing that it has great potential to adsorb uranyl ions. According to Fig (e) and (f), after the adsorption of uranyl ions, the morphology of the two kinds of adsorbents did not change greatly, and a large number of pores on the surface of the samples were filled, it is explained that uranyl ions accumulating on the samples, forming a new compound.

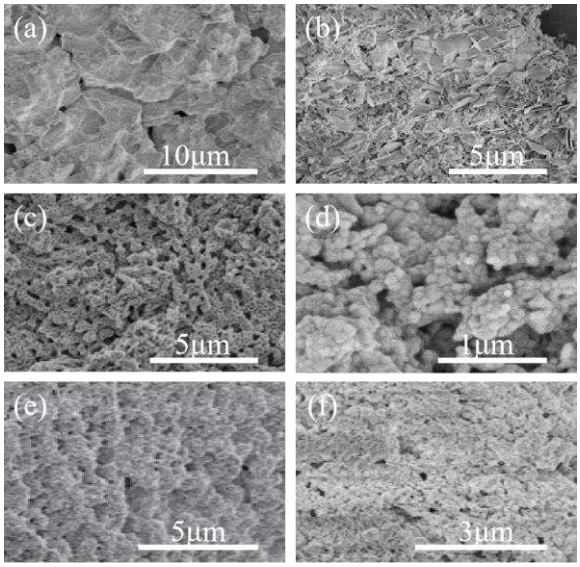


Fig 4. SEM images of $Gd_2O_3$ before (a, b) and after adsorption (e),$Gd_2O_3$-MgO before (c, d) and after adsorption (f).

The EDS energy spectra of $Gd_2O_3$ and $Gd_2O_3$-MgO showed the mass ratio of every element. As shown in Fig 5(a), the contents of Gd, O and U after $Gd_2O_3$ adsorption were 49.9%, 25.4% and 24.7%, respectively. For the used $Gd_2O_3$-MgO shown in Fig 5(b), the contents of Gd, O, Mg and U were 70.1%, 17.4%, 20.3% and 2.2%, respectively, indicating that both materials successfully adsorbed U(VI), which was consistent with the results of FT-IR and SEM analysis. It is known from the element mapping picture (Fig (c, d)) that the adsorption of uranium on the surfaces of the two kinds of materials are homogeneous distribution.

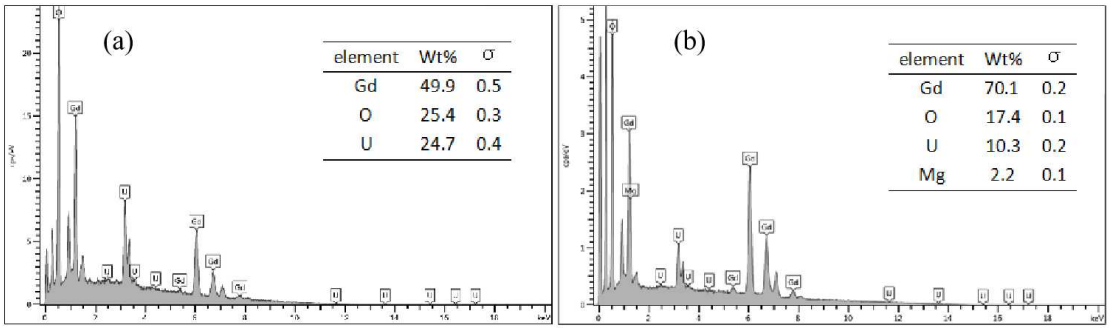

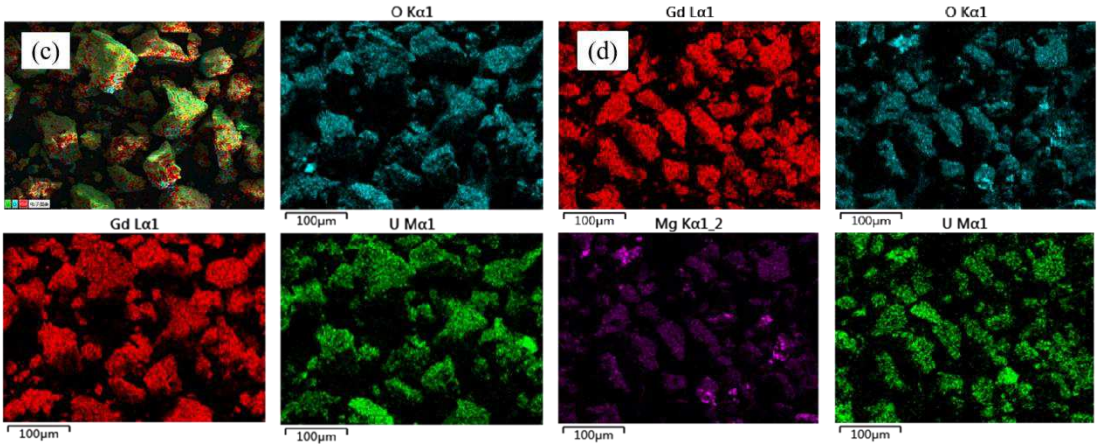


Fig 5. The EDS image and mapping picture of $Gd_2O_3$ (a, c) and $Gd_2O_3$-MgO (b, d) after adsorption of uranyl ion.

## 3.3 Adsorption property

### 3.3.1 Effect of initial pH

The pH value plays an important role in the surface properties of materials and the presence of U(VI) in aqueous solution. The effects of initial pH (3.0~ 11.0) on the adsorption properties of two kinds of materials were studied under the conditions of contact time 12 h, temperature 298K and the initial concentration of uranyl ion was 200 $mg \cdot L^{-1}$. As can be seen from Fig 6, it is obvious that the adsorption of $UO_2^{2+}$ is greatly affected by pH value. The adsorption capacity of $UO_2^{2+}$ on both materials increased as the pH increased from 3 to 6. When the pH is greater than 6, the adsorption drops sharply. Therefore, the optimal pH of the two kinds of calcined samples was 6. The existence states of U(VI) in different pH solutions are different. In the pH range of 3-6, U(VI) mainly exists in aqueous solution in the states of $UO_2^{2+}$, $(UO_2)_2(OH)_2^{2+}$, $(UO_2)_3(OH)_5^{+}$, etc. Meanwhile, hydration occurs on the surface of the material, carrying a certain amount of negative charge, which makes it easy to combine with positively charged U(VI) and its hydrolyzed products through electrostatic interaction ( Linghu et al. 2017; Oladoja et al. 2015). However, when pH is greater than 6, the existing states of uranyl ions are $(UO_2)_3(OH)^{7-}$, $UO_2(OH)^{3-}$, $UO_2(OH)_4^{2-}$, etc. These anions will repel the material surface of the negatively charged, leading to a rapid decline in adsorption capacity. (Li et al. 2015).

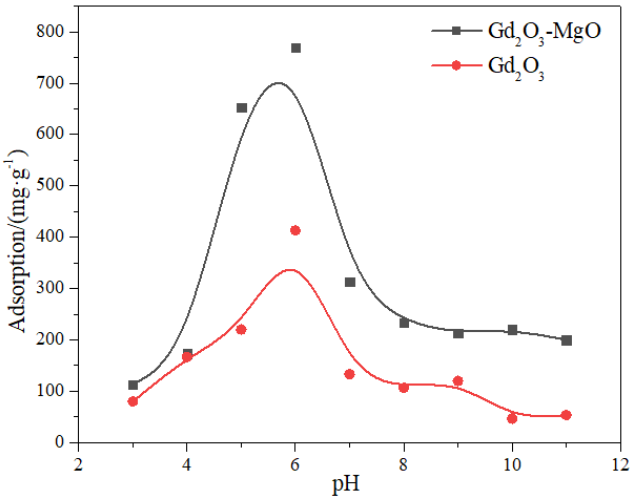


Fig 6. The influence of pH on the adsorption properties of two kinds of materials.

### 3.3.2 Adsorption isotherm

Two groups of uranium solutions with different concentrations (100, 120, 140……300 $mg \cdot L^{-1}$) of 100 mL were prepared and poured into 250 mL iodine flasks, the pH of both groups of solutions were adjusted to 6, 15mg of $Gd_2O_3$ and $Gd_2O_3$-MgO were added, respectively, and the two groups of solutions were shaken at 25℃ (180 rmp) for 12 h. The adsorption behavior of uranyl ions were described by Langmuir (2) and Fruendlich (3) equations. $R^2$ value was obtained by fitting Langmuir and Freundlich equations (Table 1), it can be seen from the table that the correlation coefficient of Langmuir equation was more suitable to describe the adsorption process of uranyl ion by adsorbents. In the Langmuir model, the surface of the adsorbent was assumed to be homogeneous ( Zhang et al. 2014). Therefore, the uniform distribution of active sites on the surface of the prepared materials may be one of the reasons for the better fit between the data and Langmuir equation, and the adsorption of $UO_2^{2+}$ on both materials is monolayer adsorption. The maximum adsorption capacities of $Gd_2O_3$ and $Gd_2O_3$-MgO calculated from the Langmuir model for $UO_2^{2+}$ are 473.43 $mg \cdot g^{-1}$ and 812.41 $mg \cdot g^{-1}$ respectively, which may be due to the synergistic effect between $Gd_2O_3$ and MgO, resulting in higher adsorption performance of $Gd_2O_3$-MgO than pure $Gd_2O_3$.

$$\frac{C_e}{Q_e} = \frac{1}{Q_0} C_e + \frac{1}{Q_0 b} \tag{2}$$

$$InQ_e = InK_F + \frac{1}{n} InC_e \tag{3}$$

Where, $C_e$ ($mg \cdot L^{-1}$) is the equilibrium concentration of the solution after the $Gd_2O_3$ and $Gd_2O_3$-MgO adsorbed uranyl ions; $Q_e$ (mg·g-1) is the equilibrium adsorption capacity of uranyl ions by unit mass of $Gd_2O_3$ and $Gd_2O_3$-MgO; $Q_0$ ($mg \cdot g^{-1}$) is the maximum adsorption capacity of the two kinds of materials for uranyl ions; b ($L \cdot mg^{-1}$) refers to the Langmuir constant, which have

relations with the affinity of the anion binding site and the adsorption-desorption energy; n and $K_F$(mg·g$^{-1}$) are Freundlich constants, which are connected with heterogeneity factor and adsorption capacity, respectively.

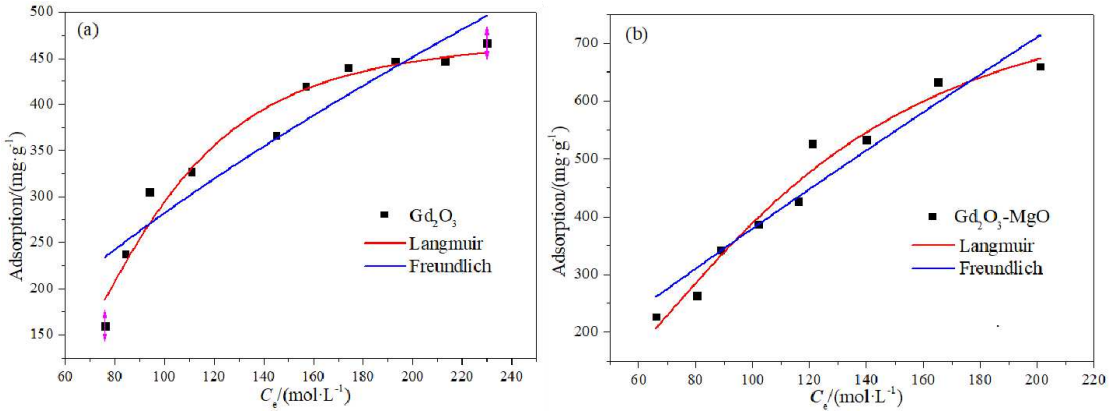


Fig 7. The influence of initial uranium concentration on adsorption properties of $Gd_2O_3$ (a) and $Gd_2O_3$-MgO (b).

Table 1.Correlation parameters of Langmuir and Freundlich isotherms.

| Adsorbent | Langmuir isotherms | | | Freundlich isotherms | | |
|---|---|---|---|---|---|---|
| | $Q_0$/(mg·g$^{-1}$) | b/(L·mg$^{-1}$) | $R^2$ | $K_F$/(mg·g$^{-1}$) | 1/n | $R^2$ |
| $Gd_2O_3$ | 473.43 | 3.73 | 0.95 | 12.43 | 0.68 | 0.87 |
| $Gd_2O_3$-MgO | 812.41 | 1.58 | 0.96 | 5.87 | 0.95 | 0.92 |

### 3.3.3 Adsorption thermodynamics

In order to explore the effect of temperature on the adsorption of $UO_2^{2+}$ by $Gd_2O_3$ and $Gd_2O_3$-MgO and to investigate the thermodynamic parameters, the adsorption experiments were arranged at 298K, 308K and 318K, respectively. The slope and intercept of the Van't Hoff equation (4) can be used to give the values of ΔH and ΔS, the Gibbs-Helmholtz equation (5) is used to calculate the value of ΔG. Table 2 shows the thermodynamic parameters. The negative values of ΔH , which indicates that the two kinds of material of uranyl ion adsorption is an exothermic process. The negative values of ΔG , which shows that the adsorption of $Gd_2O_3$ and $Gd_2O_3$-MgO to uranyl ions is spontaneous. The positive value of ΔS , which proved that the two kinds of materials of uranyl ion adsorption is the process of system chaotic degree increased. In addition, the absolute value of ΔG increases with the rising of temperature, the adsorption efficiency becomes more higher, this may be due to solute molecules in aqueous solution are moving faster at high temperature, providing the posibility of capture $UO_2^{2+}$ on the adsorbent surface (Wang et al. 2016).

$$In\frac{Q_e}{C_e} = \frac{\Delta S}{R} - \frac{\Delta H}{RT} \quad (4)$$

$$\Delta G = \Delta H - T\Delta S \quad (5)$$

Where, $Q_e$ /$C_e$ ($L \cdot g^{-1}$)is the equilibrium constant; ΔH ($kJ \cdot mol^{-1}$) is the standard enthalpy; ΔG ($kJ \cdot mol^{-1}$) is the standard Gibbs free energy; ΔS ($kJ \cdot mol^{-1}$) is the standard entropy; R is the standard gas constant (8.314 $J \cdot mol^{-1} \cdot K^{-1}$) and the temperature is T (K).

Table 2. The parameter of adsorption correlation thermodynamic.

| Temp /K | $Gd_2O_3$ | | | $Gd_2O_3$-MgO | | |
|---|---|---|---|---|---|---|
| | ΔG/($kJ \cdot mol^{-1}$) | ΔH/($kJ \cdot mol^{-1}$) | ΔS/($kJ \cdot mol^{-1} \cdot K^{-1}$) | ΔG/($kJ \cdot mol^{-1}$) | ΔH/($kJ \cdot mol^{-1}$) | ΔS/($kJ \cdot mol^{-1} \cdot K^{-1}$) |
| 298 | -20.644 | | | -86.841 | | |
| 308 | -21.009 | -9.737 | 0.0366 | -88.321 | -42.737 | 0.148 |
| 318 | -21.3758 | | | -89.801 | | |

### 3.3.4 Adsorption kinetics

Two groups of uranyl ion solution of 200 $mg \cdot L^{-1}$ were prepared, the pH was set as 6 and shaken at 25℃ (180 rmp), the supernatant was taken every certain time (0, 5, 10, 20, ……600 min) to figure out the adsorption capacity (Fig 8). The experimental data was analyzed and the adsorption rate of the reaction system was investigated by the pseudo-first-order kinetic model (6) and the pseudo-second-order kinetic model (7). According to the analysis of adsorption kinetics, the adsorption capacity of $Gd_2O_3$ increases rapidly before 90 min, then becomes flat, and finally reaches the adsorption equilibrium around 180 min. After doping MgO, the adsorption capacity of the $Gd_2O_3$-MgO was significantly improved, and reached the adsorption equilibrium of the material about 300 minutes. The adsorption process of uranyl ions by two kinds of materials were more suitable to be fitted by pseudo-second-order kinetic model, which is mainly controlled by chemisorption (Yunsheng et al. 2017).

$$In(Q_e - Q_t) = InQe - k_1 t \quad (6)$$

$$\frac{t}{Q_t} = \frac{1}{k_2 Q_e^2} + \frac{t}{Q_e} \quad (7)$$

Where, $Q_e$ ($mg \cdot g^{-1}$) is the equilibrium adsorption capacity of $Gd_2O_3$ and $Gd_2O_3$-MgO to uranyl ions; $Q_t$ ($mg \cdot g^{-1}$) is the adsorption capacity of two kinds of materials at any time t; The rate constants of pseudo-first-order and pseudo-second-order adsorption kinetics models are $k_1$ ($min^{-1}$)

and $k_2$ ($g \cdot mg^{-1} \cdot min^{-1}$), respectively.

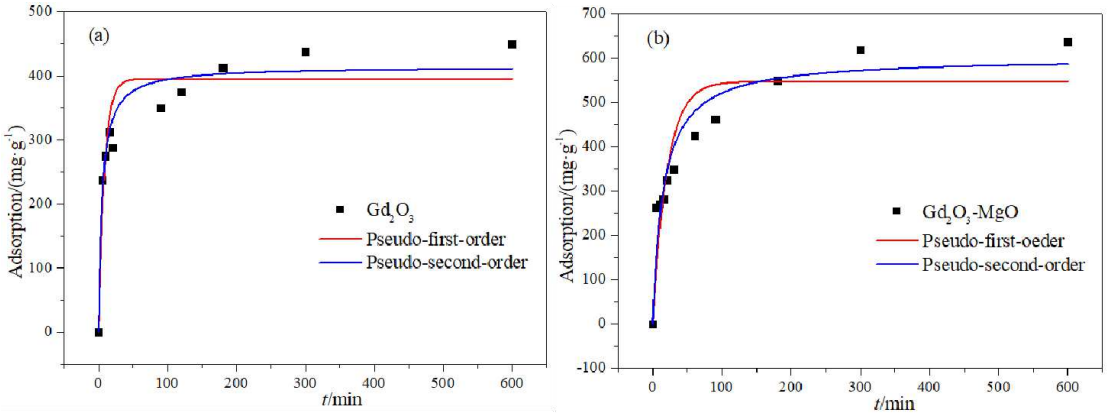


Fig. 8. The influce of contact time on the adsorption properties of $Gd_2O_3$ (a) and $Gd_2O_3$-MgO (b).

Table 3. Correlation parameters of pseudo-first-order and pseudo-second-order models .

| Adsorbent | Pseudo-first-order model | | | Pseudo-second-order model | | |
|---|---|---|---|---|---|---|
| | $Q_e/(mg \cdot g^{-1})$ | $K_1/(min^{-1})$ | $R^2$ | $Q_e/(mg \cdot g^{-1})$ | $K_2/(g \cdot mg^{-1} \cdot min^{-1})$ | $R^2$ |
| $Gd_2O_3$ | 395.24 | 0.12 | 0.88 | 414.65 | $4.72\times10^{-4}$ | 0.94 |
| $Gd_2O_3$-MgO | 547.55 | 0.05 | 0.81 | 602.23 | $1.07\times10^{-4}$ | 0.91 |

### 3.3.5 Comparison of uranyl adsorption capacity between two kinds of materials and other adsorbents.

Table 4 lists the adsorption properties of several different adsorbents for uranyl ions. As can be seen from the table, there are good uranyl ion adsorption effect on the preparation of the two kinds of adsorbents, the adsorption effect of $Gd_2O_3$-MgO is more significant, it also suggests that the composite oxide on the adsorption of uranyl ion in wastewater has a certain application prospect.

Table 4. Adsorption properties of uranyl ions on different adsorbents.

| Adsorbents | pH | Adsorption capacity/(mg·g$^{-1}$) | References |
|---|---|---|---|
| UiO-66-TBP | 5 | 201.9 | (Rajaei et al. 2021) |
| AO/g-$C_3N_4$ | 6.8 | 312 | (Hu et al. 2021) |
| 3D AFC | 5.8 | 127.5 | (Song et al. 2021) |
| TCHC | 5.5 | 96.99 | (Wang et al. 2020) |
| PCP-$NH_2$ | 5 | 274.2 | (Xie et al. 2020) |
| Iron/carbon composites | 4 | 105.3 | (Li et al. 2020) |
| Polypropylene nanofibers | 4 | 83.24 | (Ashrafi et al. 2019) |
| AMD | 5 | 493.6 | (Bayramoglu et al. 2016) |
| Gelatin-FeS | 5 | 555.9 | (Shao et al. 2016) |
| $Gd_2O_3$ | 6 | 473.43 | This work |
| $Gd_2O_3$-MgO | 6 | 812.41 | This work |

## 3.5 Possible adsorption mechanism

In order to study the possible mechanism of adsorption for uranyl ions by $Gd_2O_3$ and $Gd_2O_3$-MgO, XPS was used to analyze the adsorbent (Fig 9). Figure (a) and (c) completely show the full range of XPS images of the two kinds of materials. In the fresh and used materials, Gd4d, O1s and C1s all exist in the spectral peaks. By comparing the two figures (a) and (c), it can be seen that Mg2p exists in $Gd_2O_3$-MgO material, indicating that Mg element is successfully doped into $Gd_2O_3$ material. In Figure (b) and (d), the peaks at ~381.0eV and ~392.0eV belong to the characteristic peaks of $U4f_{7/2}$ and $U4f_{5/2}$, indicating that both $Gd_2O_3$ and $Gd_2O_3$-MgO successfully capture uranium in aqueous solution, and this result was also verified by EDS and FT-IR analysis ( Llton et al.2011). For the two kinds of materials, their C1s and O1s peaks can be clearly seen. The characteristic peak of C1s is shown in Fig. (e) (g). The energy allocated to the C1s spectrum is calibrated by combining the peak of ~284.8eV. The peak of binding energy ~289eV is attributed to the carbon atoms in carbonate, which is generated by the reaction of $H_2O$ and $CO_2$ on the surface of the absorbent (Yunsheng et al. 2017). The characteristic peaks of O1s are shown in Figure (f) (h). The line of O1s at ~530 eV can be allocated to the oxygen in the oxide (M-O) (Qiu et al. 2008), the peak at ~531 eV is related to the oxygen in the hydroxyl group (-OH) (Shahbazi et al. 2011), and the peak of binding energy at ~ 532 eV is allocated to the oxygen in the water ($H_2O$). (Wang et al. 2016). Hydroxyl groups were generated in the surface hydration of the material when it contacts water, this is the reason for the characteristic peaks of $H_2O$ and -OH included in the

results (Wang et al. 2018). Compared with the sample before adsorption,the -OH groups content of $Gd_2O_3$ and $Gd_2O_3$-MgO decrease from 21.75% ,17.42% to 12.82%, 12.85% after $UO_2^{2+}$ adsorption, demonstrating that the hydroxyl group generated by the surface hydration of the adsorbent was involved in the adsorption process of U(VI). The adsorption is mainly through the hydroxylation of functional groups on the surface of the adsorbents and the hydroxylated products were complexed with uranyl ion to finish adsorption process. The possible adsorption process is shown in Fig 10.

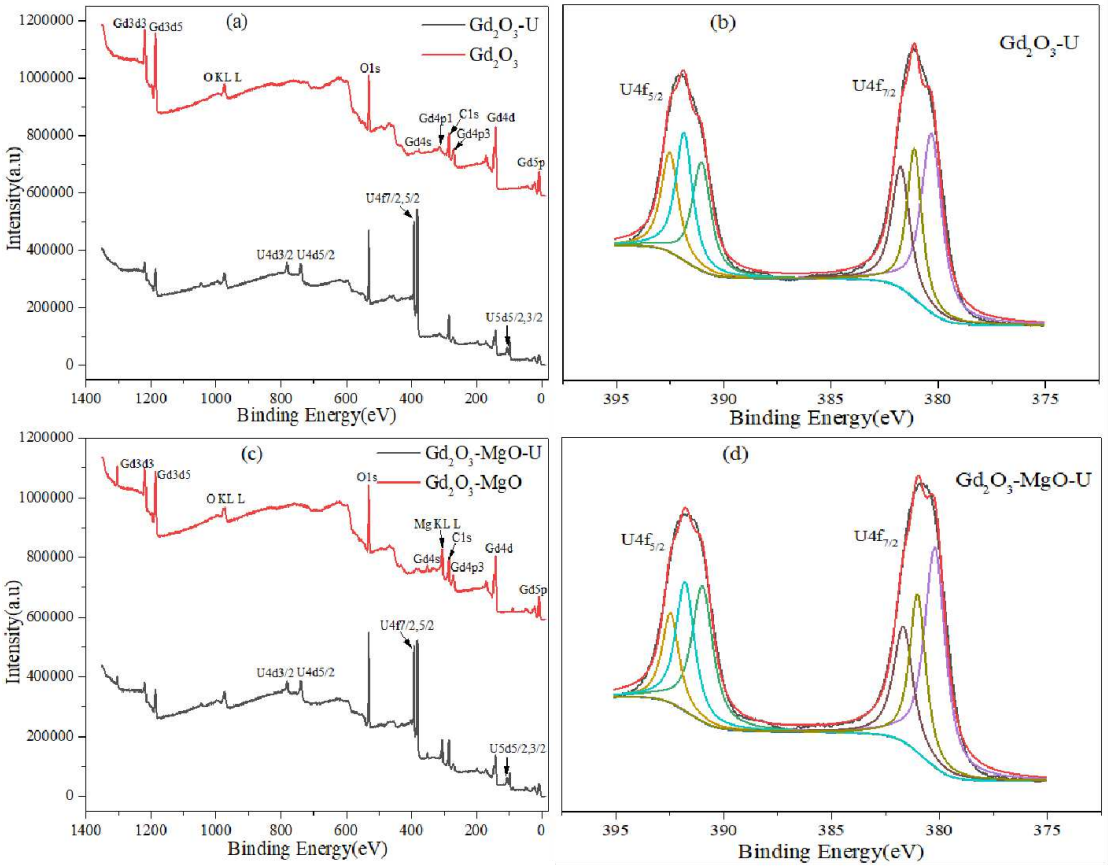

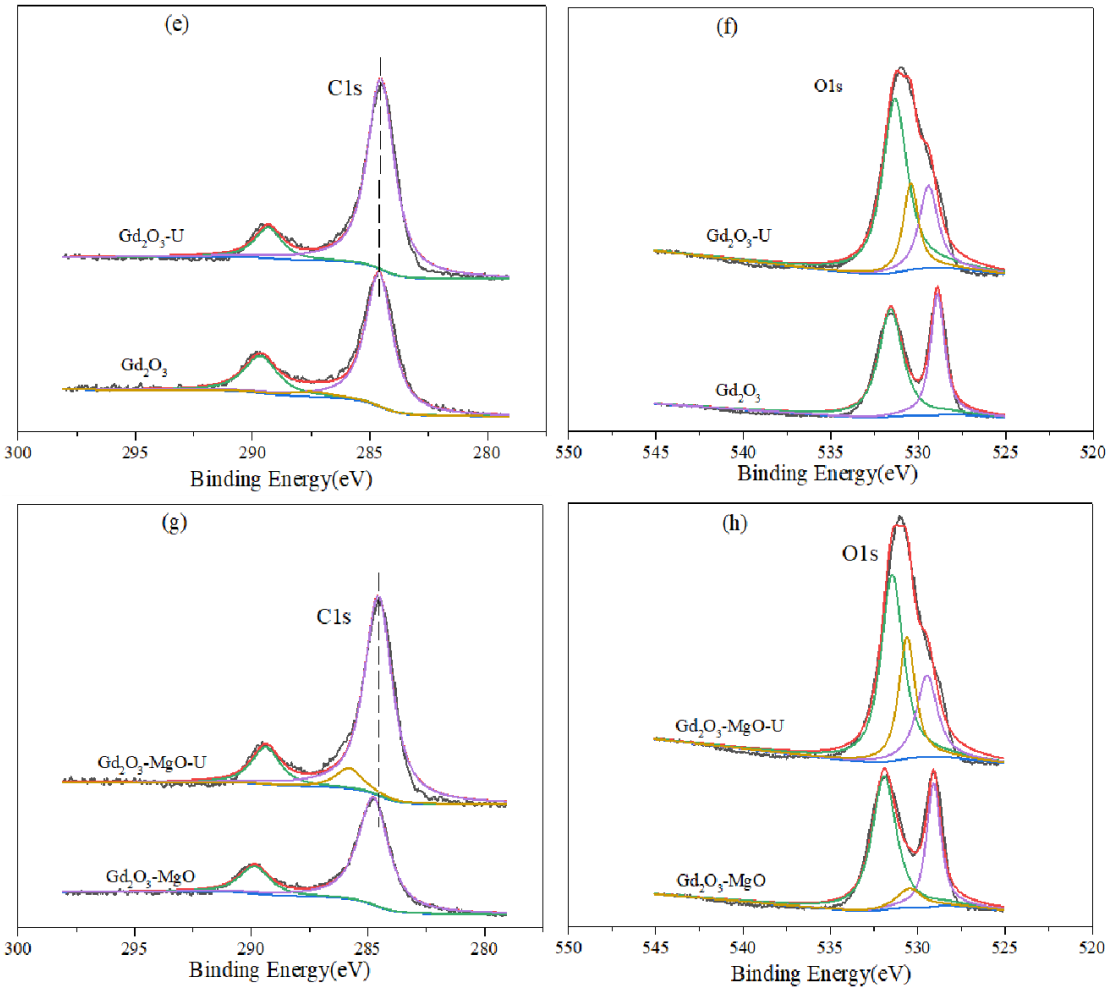


337

338 Fig 9. XPS spectra of $Gd_2O_3$ and $Gd_2O_3$-MgO.

339

340 .

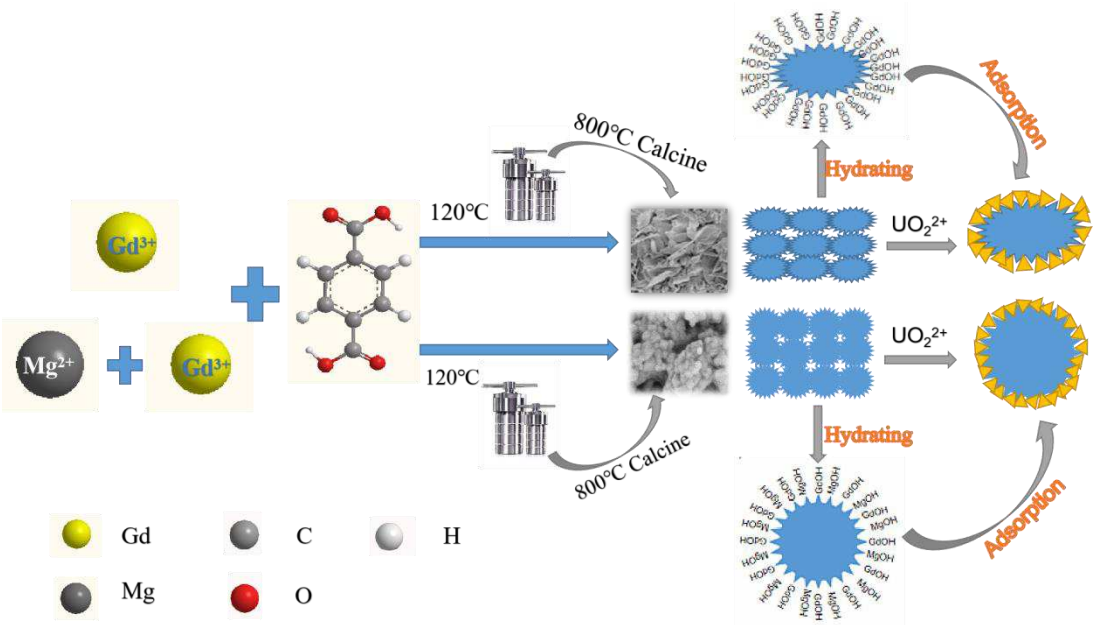


Fig 10. The surface adsorption of adsorbent for U(VI).

## 4 Conclusion

In conclusion, pure $Gd_2O_3$ and $Gd_2O_3$-MgO composites were successfully prepared by hydrothermal method and calcination treatment. The crystal morphology and structure of the two kinds of samples were representated by XRD, FT-IR, SEM, EDS and XPS, the synthesized materials have typical cubic crystal structure. The adsorption experiments showed that materials have a good remove performence for U(VI). When the molar ratio of $Gd(NO_3)_3 \cdot 6H_2O/Mg(NO_3)_2 \cdot 6H_2O$ is 1:1, the composite has the best crystallinity and the largest adsorption capacity for uranyl ions. Compared with the pseudo-fisrt-order model, the adsorption kinetics can be better reflected by the pseudo-second -order model, and the adsorption isotherm can be reproduced by the Langmuir equation for the two kinds of materials. The $Gd_2O_3$ obtained the maximum adsorption capacities of 473.43 $mg \cdot g^{-1}$ and $Gd_2O_3$-MgO got 812.41 $mg \cdot g^{-1}$. Thermodynamic analysis of adsorption further shows that the adsorption process of $Gd_2O_3$ and $Gd_2O_3$-MgO for U(VI) are spontaneous and exothermic. Under these circumstances, the adsorption mechanism of uranium is chiefly due to the surface hydroxylation of the adsorbent in aqueous solution to produce Gd-OH and Mg-OH, and the complexation of surface -OH and uranyl ions.

## Declarations

## Ethics approval and consent to participate Not applicable.

## Consent for publication

All authors have consented to this content and have expressly consented to its publication.

## Availability of data and materials

Not applicable.

## Competing interests

The authors declare no conflict of interest.

## Finding

The work was suported by the National Natural Science Foundation of China(21667024).

## Authors'contributions

All authors contributed to the concept and design of the study. Lili Zhang: preparation and completion of experiments, data analysis, manuscript preparation and writing; Yuantao Chen*: methodological analysis; Meng Zhao: experiment preparation; Wang Yinghui: Review of the original draft.

## Acknowledgements

Thanks to the National Natural Science Foundation for its support.

## References

Abudief A M, Essawy A A, Diab A K et al. (2020) Facile Synthesis and Characterization of Novel $Gd_2O_3$/CdO Binary Mixed Oxide Nanocomposites of Highly Photocatalytic Activity for Wastewater Remediation under Solar Lumination[J]. Journal of Physics and Chemistry of Solids 148

Abu-Dief AM (2020) Development of metal oxide nanoparticles as semiconductors[J]. Nanotechnol Nanomaterials 1(1):5–10

Ashrafi F, Firouzzare M, Ahmadi S J et al. (2019) Preparation and modification of forcespun polypropylene nanofibers for adsorption of uranium (VI) from simulated seawater[J]. Ecotoxicology and Environmental Safety 186:109746

Bayramoglu G, Arica M Y (2016) MCM-41 silica particles grafted with polyacrylonitrile: Modification in to amidoxime and carboxyl groups for enhanced uranium removal from aqueous medium[J]. Microporous and Mesoporous Materials 226:117-124

Cheng Xu, Wei Zhang, Yuantao Chen et al. (2019) Synthesis of $NH_2$ -MIL-125/$NH_2$ -MIL-125-P@$TiO_2$ and Its Adsorption to Uranyl Ions[J]. Chemistry Select 43(04):12801-12806

Choi J S, Lingamdinne L P, Yang J K et al. (2020) Fabrication of chitosan/graphene oxide-gadolinium nanorods as a novel nanocomposite for arsenic removal from aqueous solutions[J]. Journal of Molecular Liquids 320:114410

Chowdhury I H, Chowdhury A H, Bose P et al. (2016) Effect of anion type on the synthesis of mesoporous nanostructured MgO, and its excellent adsorption capacity for the removal of toxic heavy metal ions from water[J]. Rsc Advances 6(8):6038-6047

Chowdhury A H, Chowdhury I H, Naskar M K et al. (2015) A facile synthesis of grainy rod-like porous MgO[J]. Mater. Lett. 158:190-193

Dhananjaya N, Nagabhushana H, Sharma S et al. (2014)Hydrothermal synthesis of $Gd_2O_3$:$Eu^{3+}$ nanophosphors: Effect of surfactant on structural and luminescence properties[J]. Journal of Alloys and Compounds 587: 755-762

Fei Hailong, Liu Xin, Li Zhiwei et al. (2015) Synthesis of manganese coordination polymer microspheres for lithium-ion batteries with good cycling performance[J]. Electrochimica Acta 174:1088-1095

Han Y, Zhang S, Shen N et al. (2016) MOF-derived porous NiO nanoparticle architecture for high performance supercapacitors[J]. Materials Letters S0167577X16315117

He F, Yang P, Wang D et al. (2011) Preparation and up-conversion luminescence of hollow $La_2O_3$:Ln (Ln = Yb/Er, Yb/Ho) microspheres[J]. Langmuir 27(9): 5616-23

Huang C-C, Liu T-Y, Su C-H et al. (2008) Superparamagnetic hollow and paramagnetic porous $Gd_2O_3$ particles[J]. Chemistry of Materials 20(12): 3840-3848

Hu B, Wang H, Liu R et al. (2021) Highly efficient U(VI) capture by amidoxime/carbon nitride composites: Evidence of EXAFS and modeling[J]. Chemosphere 274:129743

Jiu H, Jia W, Zhang L et al. (2015) Synthesis, luminescent and drug-release properties of $SiO_2$@$Y_2O_3$:Eu hollow mesoporous microspheres[J]. Journal of Porous Materials 22(6): 1511-1518

Juibari N M, Tarighi S (2020) Metal–organic framework-derived nanocomposite metal-oxides with enhanced catalytic performance in thermal decomposition of ammonium perchlorate[J]. Journal of Alloys and Compounds 832

Kaura R, Kaura A, Umar A et al. (2019) Metal organic framework (MOF) porous octahedral nanocrystals of Cu-BTC: Synthesis, properties and enhanced adsorption properties[J]. Materials Research Bulletin 109(1): 124-133

Liu M, Luo J, Li F et al. (2016) Adsorption equilibrium and kinetics of uranium onto porous azo-metal-organic frameworks[J]. Radioanal Nucl Chem 310:1-10

Li M X, Liu H B, Chen T H et al. (2020) Effificient U(VI) adsorption on iron/carbon composites derived from the coupling of cellulose with iron oxides: Performance and mechanism[J]. Sci.Total Environ 703:135604

Liu P, Yu Q, Xue Y et al. (2020) Adsorption performance of U(VI) by amidoxime-based activated carbon[J]. Radioanal Nucl Chem 324:813–822

Li W, Chen D, Xia F et al. (2015) Extremely high arsenic removal capacity for mesoporous aluminium magnesium oxide composites[J]. Environ Sci Nano 3:94–106

Llton E S, Bagus P S (2011) XPS determination of uranium oxidations states[J]. Surf. Interface Anal 43:275–286

Luo B C, Yuan L Y, Chai Z F et al. (2016) U(VI) capture from aqueous solution by highly porous and stable MOFs: UiO-66 and its amine derivative[J]. Journal of Radioanalytical and Nuclear Chemistry 307(1):269-276

Lin M C, Chang F T, Uan J Y et al. (2013) Aqueous $Li^{+}/Al^{3+}$ alkaline solution for $CO_2$ capture and the massive Li-Al-$CO_3$ hydrotalcite precipitation during the interaction between $CO_2$ gas and the $Li^{+}/Al^{3+}$ aqueous solution[J]. Mater. Chem 46:14773–14782

Linghu W, Yang H, Sun Y et al. (2017) One-pot synthesis of LDH/GO composites as highly effective adsorbents for decontamination of U(IV)[J]. ACS Sustain. Chem. Eng 5:5608 -5616

Molavi H, Eskandari A, Shojaei A et al. (2018) Enhancing $CO_2/N_2$ adsorption selectivity via post-synthetic modification of $NH_2$-UiO-66 (Zr)[J]. Microporous and Mesoporous Materials 257: 193-201

Mohamed W S, Abu-Dief, Ahmed et al. (2018) Synthesis, characterization and photocatalysis enhancement of $Eu_2O_3$-ZnO mixed oxide nanoparticles[J]. The journal of physics and chemistry of solids 116:375-385

Muneer I, Farrukh M A, Javaid S et al. (2015) Synthesis of $Gd_2O_3/Sm_2O_3$ nanocomposite via sonication and hydrothermal methods and its optical properties[J]. Superlattices and Microstructures 77:256-266

Oladoja, N A, Chen S, Drewes J E et al. (2015) Characterization of granular matrixsupported nano magnesium oxide as an adsorbent for defluoridation of groundwater [J]. ChemicalEngineering Journal 281(3): 632-643

Peng W, Huang GL, Yang SS, et al. (2019) Performance of biopolymer/graphene oxide gels for the effective adsorption of U(VI) from aqueous solution[J]. Radioanal Nucl Chem 322:861–868

Trejo-García P, Palomino-Merino R, Cruz J et al. (2020) Luminescent properties of titania doped with nanoparticles of gadolinium oxide and europium[J]. Ceramics International 46(16):26326-26334

Qian B, Zou H, Meng D et al. (2018) Columnar $Gd_2O_3:Eu^{3+}/Tb^{3+}$ phosphors: preparation, luminescence properties and growth mechanism[J]. CrystEngComm 20(45):7322-7328

Qiu L. G, Li Z. Q, Wu Y et al. (2008) Facile synthesis of nanocrystals of a microporous metal–organic framework by an ultrasonic method and selective sensing of orgaoamines[J]. Chem. Commun 3642-3644

460 Rajaei A, Ghani K, Jafari M (2021) Modification of UiO-66 for removal of uranyl ion from
461 aqueous solution by immobilization of tributyl phosphate[J]. Journal of Chemical Sciences
462 133(1):14

463 Shahbazi A. (2011) Functionalized SBA-15 mesoporous silica by melamine-based dendrimer
464 amines for adsorptive characteristics of Pb(II), Cu(II) and Cd(II) heavy metal ions in batch
465 and fixed bed column[J]. Chemical Engineering Journal 168(2): 505-518

466 Shao D, Ren X, Wen J et al. (2016) Immobilization of uranium by biomaterial stabilized FeS
467 nanoparticles: effects of stabilizer and enrichment mechanism[J]. Hazard. Mater 302 (2016)
468 1–9

469 Song F, Zhang Z, Mai X et al. (2021) Efficient removal of U(VI) from aqueous solutions via an
470 activated 3D framework carbon[J]. Journal of Radioanalytical and Nuclear Chemistry
471 327(2):721-729

472 Syrbua N, Zalamaia I V, Culeacb M et al. (2019) Optical activity induced by rare-earth ions in
473 $As_2S_3$ glasses and KCl crystals[J]. Optics and Laser Technology 114: 216-223

474 Tamrakar R K, Bisen D. (2015) Thermo luminescence studies of ultraviolet and gamma irradiated
475 erbium(III)-and ytterbium(III)-doped gadolinium oxide phosphors[J]. Materials Science in
476 Semiconductor Processing 33: 169-188

477 Tarighi S, A Bb Asi A, Geranmayeh S et al. (2013) Synthesis of a new interpenetrated mixed
478 ligand Ni (II) metal organic framework: structural, thermal and fluorescence studies and its
479 thermal decomposition to NiO nanoparticles[J]. Inorg. Organomet. Polym. Mater
480 23(4):808-815

481 Wang De, Xu Yanbin, Difei et al. (2019) Ultra-thin iron phosphate nanosheets for high efficient
482 U(VI) adsorption[J]. Journal of Hazardous Materials 371:83-93

483 Wang F, Li H, Liu Q et al. (2016) A graphene oxide/amidoxime hydrogel for enhanced uranium
484 capture[J]. Sci. Rep 6:19367

485 Wang J , Fang F, Zhou Y et al. (2020) Facile modification of graphene oxide and its application
486 for the aqueous uranyl ion sequestration: Insights on the mechanism[J]. Chemosphere
487 258:127152

488 Wang X, Fan Q, Yu S et al. (2016) High sorption of U(VI) on graphene oxides studied by batch
489 experimental and theoretical calculations [J]. Chemical Engineering Journal 287: 448-455

490 Wang X , Lan L , Alvarez P et al. (2015) Synthesis and characterization of green agents coated
491 Pd/Fe bimetallic nanoparticles[J]. Journal of the Taiwan Institute of Chemical Engineers
492 50(10n11):297-305

493 Wang XL, Guo HX, Wang F et al. (2020) Halloysite nanotubes: an eco-friendly adsorbent for the
494 adsorption of Th(IV)/U(VI) ions from aqueous solution[J].Radioanal Nucl Chem 324:1151–
495 1165

496 Wang Y, Chen Y, Liu C et al. (2018) High-efficiency enrichment of uranium(VI) from aqueous
497 solution by hydromagnesite and its calcination products[J]. Journal of Radioanalytical and
498 Nuclear Chemistry 315:171-183

499 Wang Z, Liu Z, Ye T et al. (2020) Removal of uranyl ions from aqueous media by tannic
500 acid-chitosan hydrothermal carbon: equilibria, kinetics and thermodynamics[J]. Journal of
501 Radioanalytical and Nuclear Chemistry 326:1843-1852

502 Xie X, Wang Y, Xiong Z et al. (2020) Highly efficient removal of uranium(VI) from aqueous
503 solution using poly(cyclotriphosphazene- co -polyethyleneimine) microspheres[J]. Journal of
504 Radioanalytical and Nuclear Chemistry 326(3):1867-1877

505 Yan L, Xu Y, Yang W et al. (2018) MOF-Derived Metal Oxide Composites for Advanced
506 Electrochemical Energy Storage.[J]. Small 14(25):1704435

507 Yang H, Luo XG, Ding HL et.al. (2019) Adsorption of U(VI) by Elodea nuttallii: equilibrium,
508 kinetic and mechanism analysis[J]. Radioanal Nucl Chem 319:227–235

509 Yao N, Fan Z, Meng R et al. (2020) A cobalt hydroxide coated metal-organic framework for
510 enhanced water oxidation electrocatalysis[J]. Chemical Engineering Journal 127319

511 Yunsheng, Wang, Yuantao Chen, Fang Yu et al. (2017) The effect of magnesium oxide
512 morphology on adsorption of U(VI) from aqueous solution[J]. Chemical Engineering Journal
513 316:936-950

514 Zhao CS, Liu J, Deng YH et al. (2019) Uranium(VI) adsorption from aqueous solutions by
515 microorganism-graphene oxide composites via an immobilization approach[J]. Clean Prod
516 236:117624

517 Zhang B, Sun HY, Li J et al. (2019) Fast and selective removal of aqueous uranium by a
518 $K^+$-activated robust zeolitic sulfde with wide pH resistance[J].Inorg Chem 58:11622–11629

519 Zhang Y, Lu X, Lin et al. (2014) Removal of fluoride from groundwater by adsorption onto La
520 (III)-Al (III) loaded scoria adsorbent[J]. Appl. Surf. Sci 303:1–5

521 Zhydachevskyy, V. Tsiumra, M. Baran, L et al. (2018) Quantum efficiency of the
522 down-conversion process in $Bi^{3+}$–$Yb^{3+}$co-doped $Gd_2O_3$[J]. Luminescence 196:169-173

# Figures

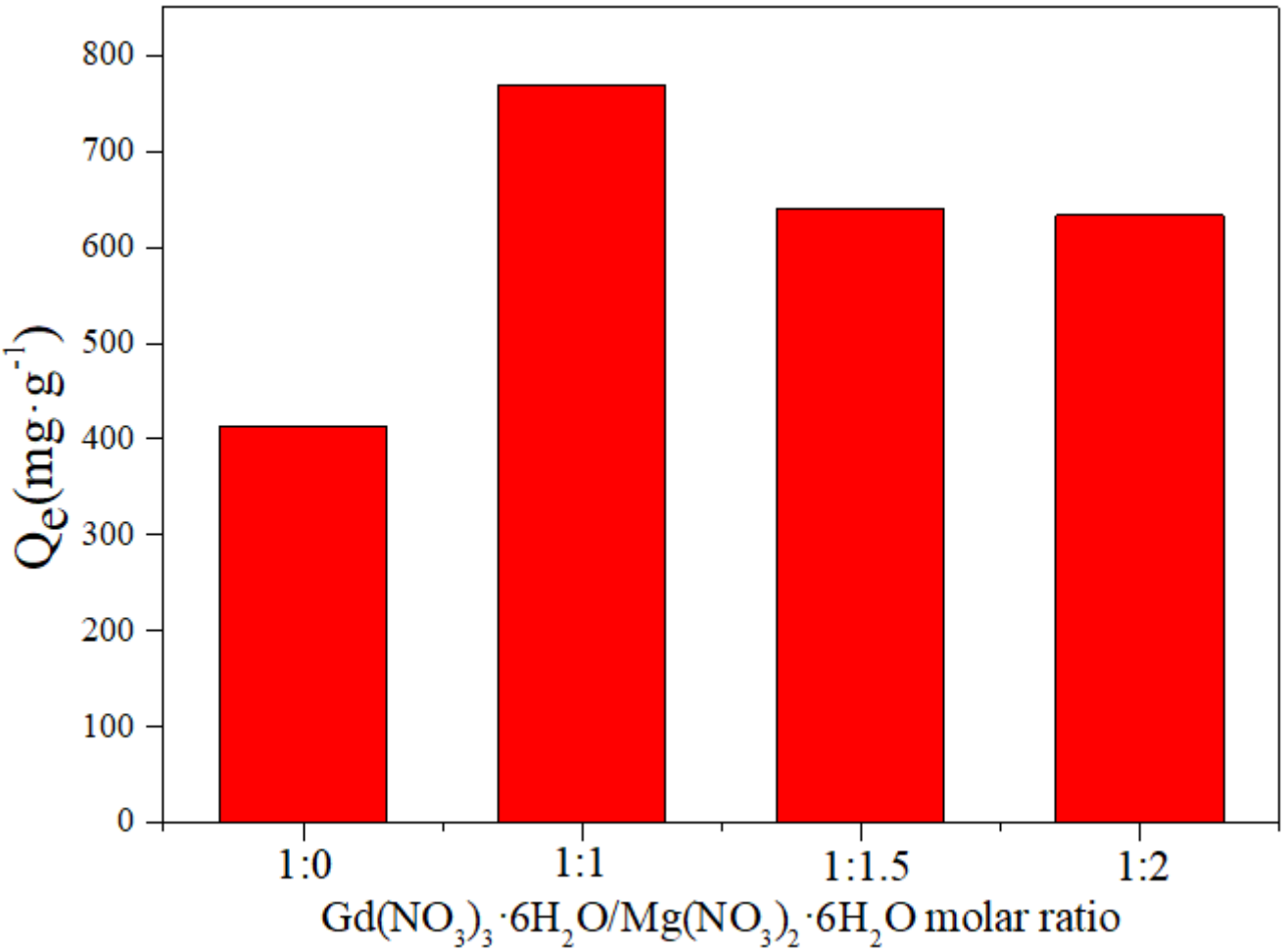


**Figure 1**

Effect of Gd(NO3)3·6H2O/Mg(NO3)2·6H2O molar ratio on UO22+ adsorption.

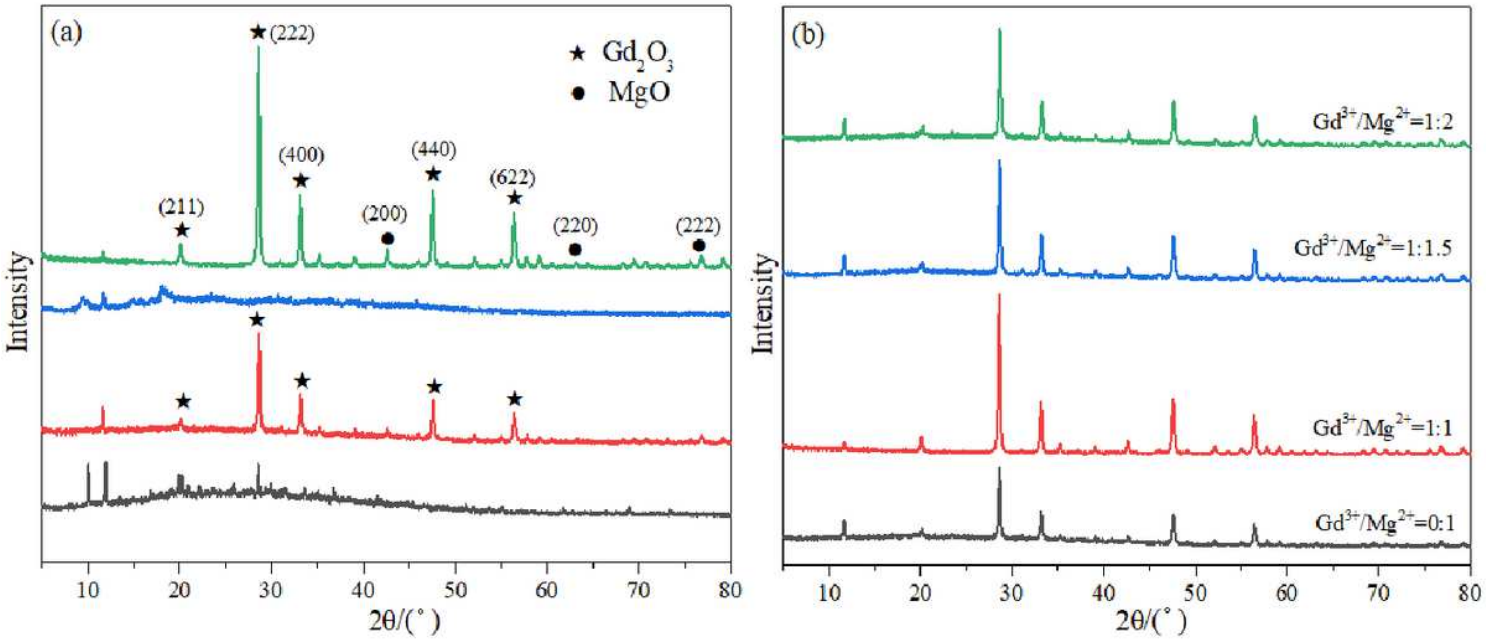

## Figure 2

XRD patters (a) of two kinds of materials and their precursors and (b) of Gd2O3-MgO with different Gd(NO3)3·6H2O/Mg(NO3)2·6H2O molar ratio.

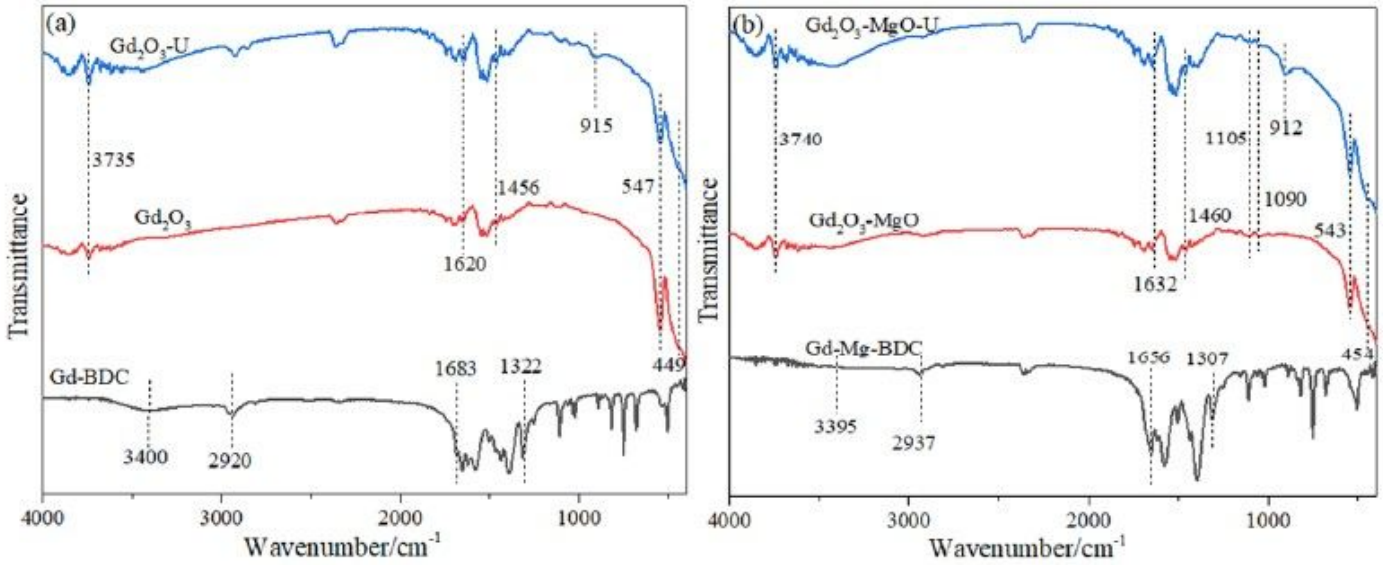


## Figure 3

FT-IR spectra of Gd2O3 (a) and Gd2O3-MgO (b) before and after adsorption and their precursor.

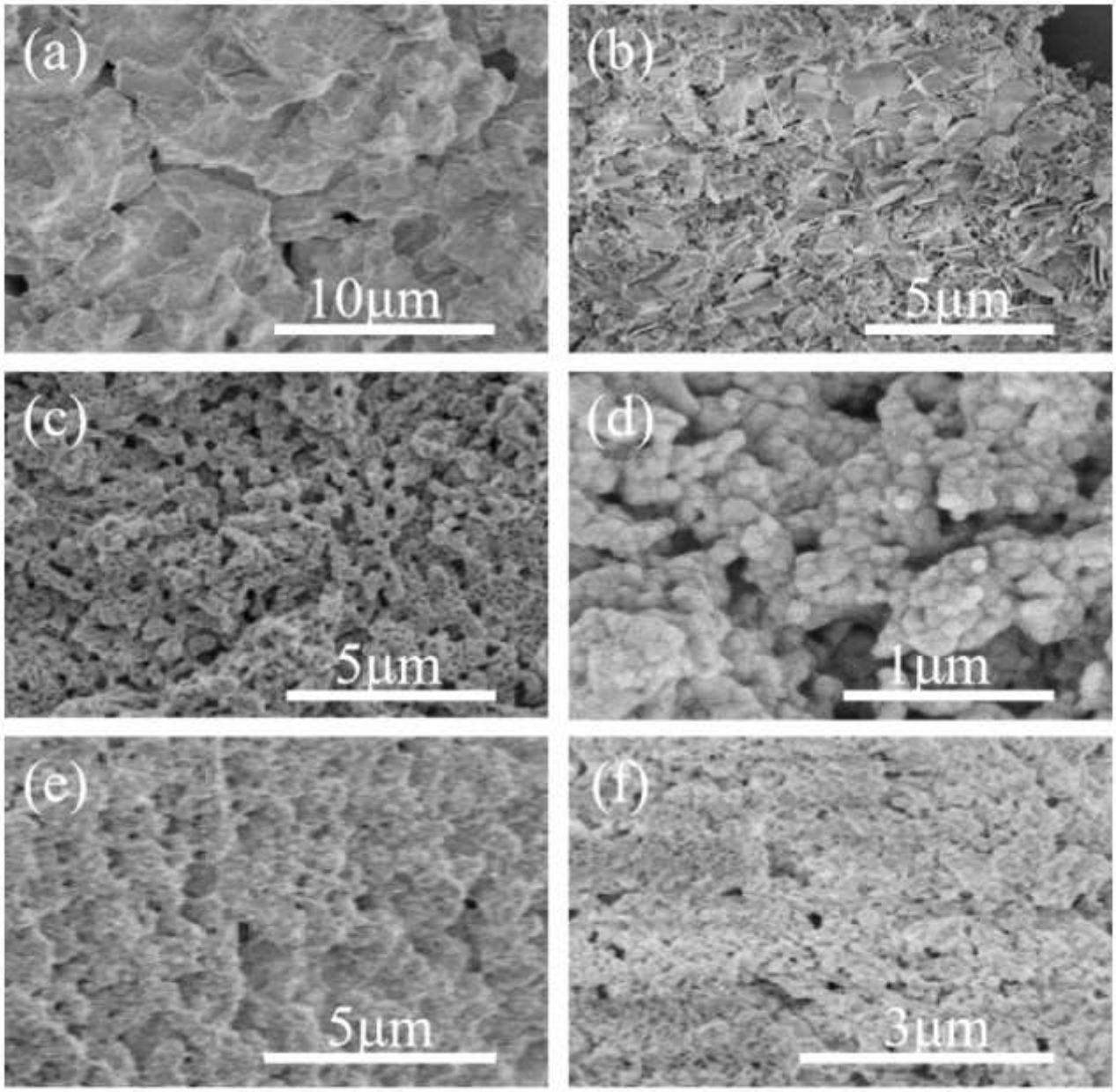


**Figure 4**

SEM images of Gd2O3 before (a, b) and after adsorption (e),Gd2O3-MgO before (c, d) and after adsorption (f).

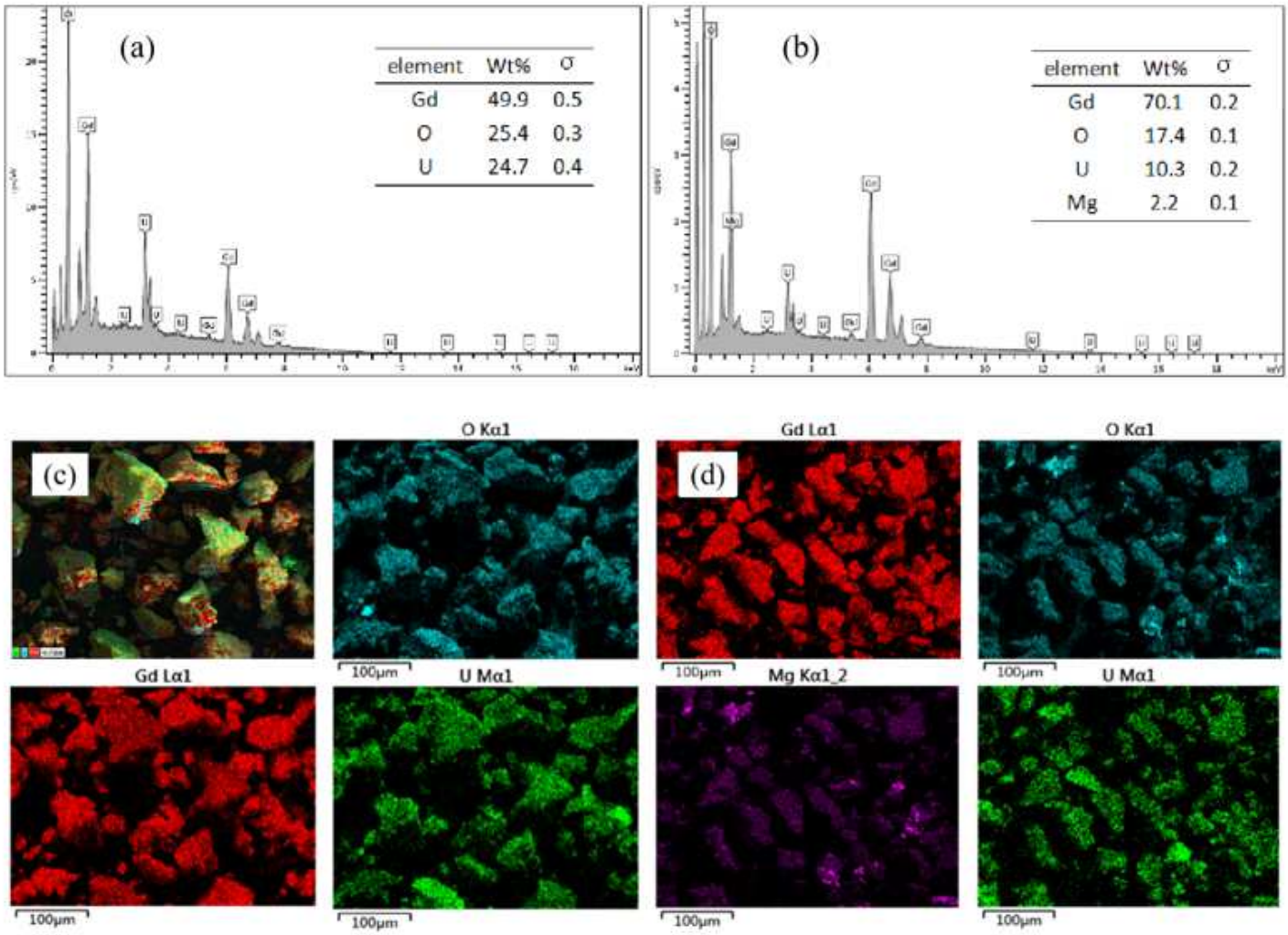


## Figure 5

The EDS image and mapping picture of Gd2O3 (a, c) and Gd2O3-MgO (b, d) after adsorption of uranyl ion.

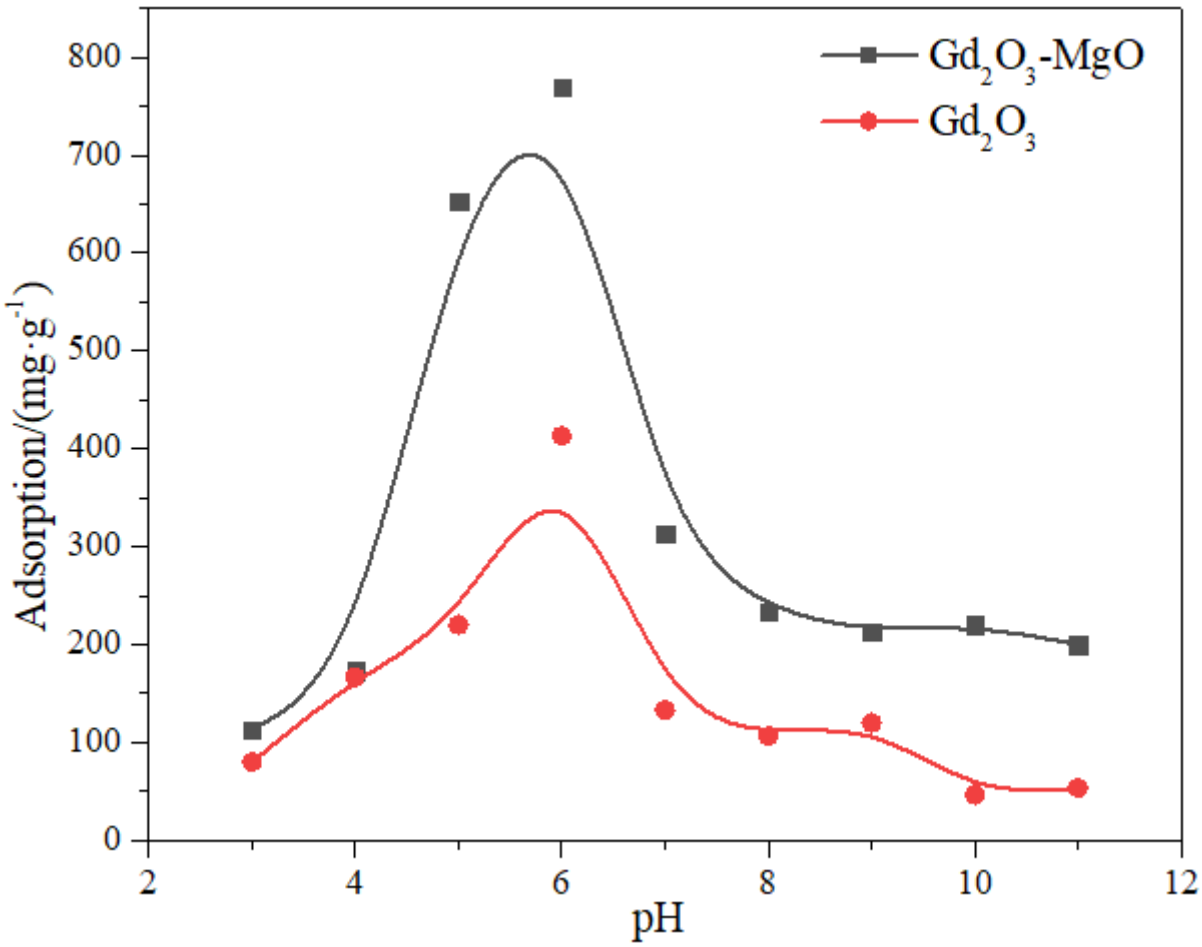


**Figure 6**

The influence of pH on the adsorption properties of two kinds of materials.

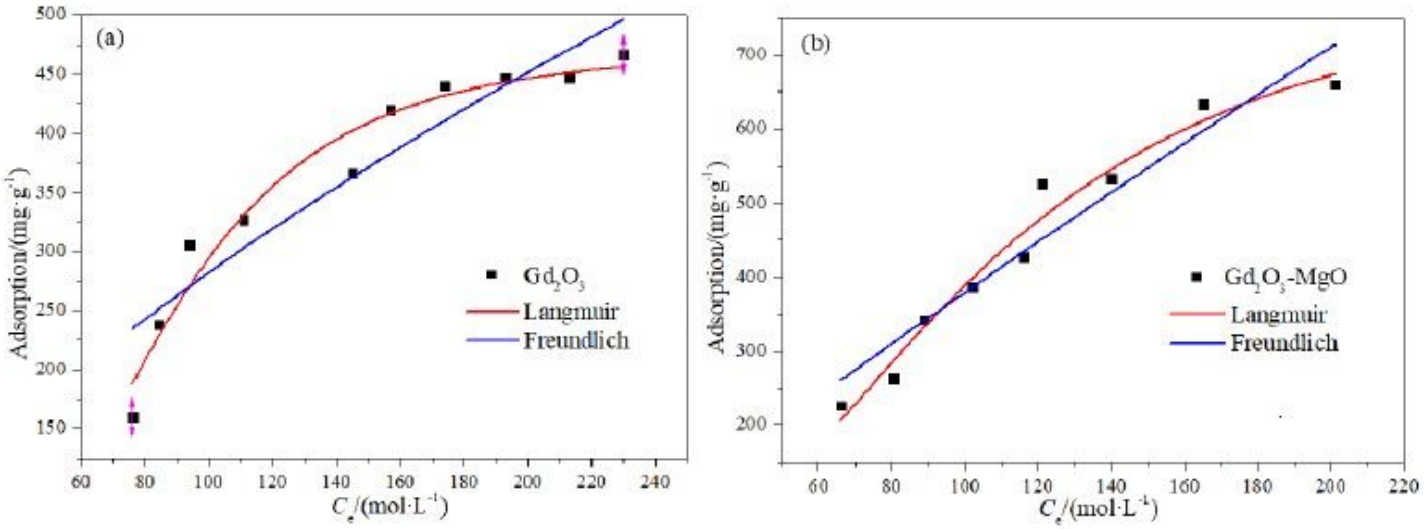


**Figure 7**

The influence of initial uranium concentration on adsorption properties of Gd2O3 (a) and Gd2O3-MgO (b).

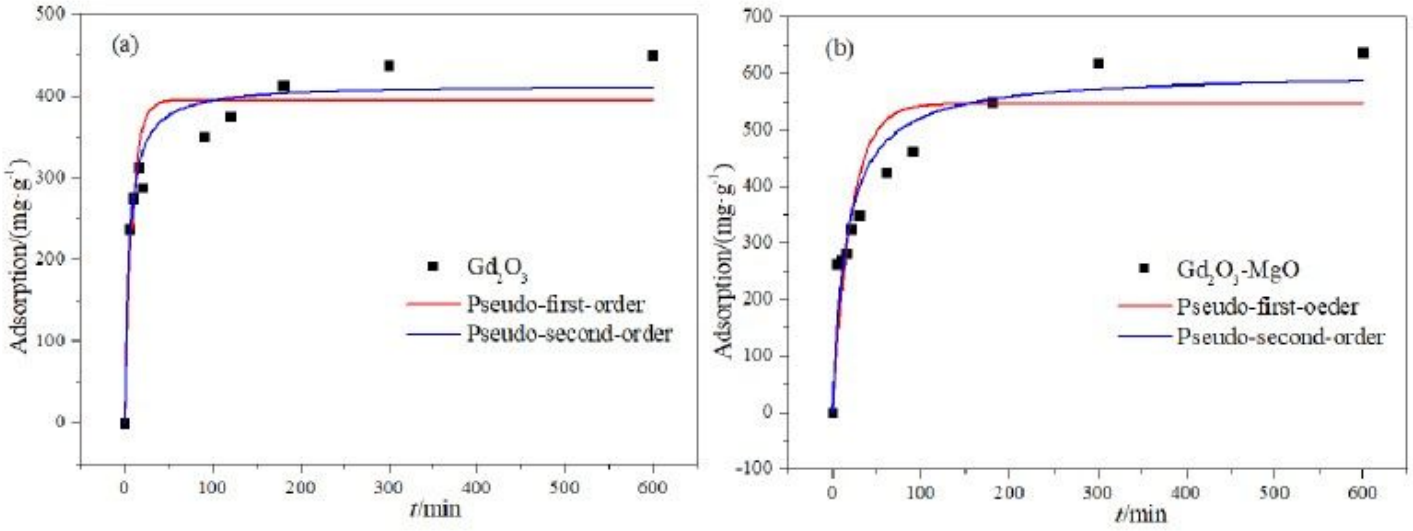


**Figure 8**

The influce of contact time on the adsorption properties of Gd2O3 (a) and Gd2O3-MgO (b).

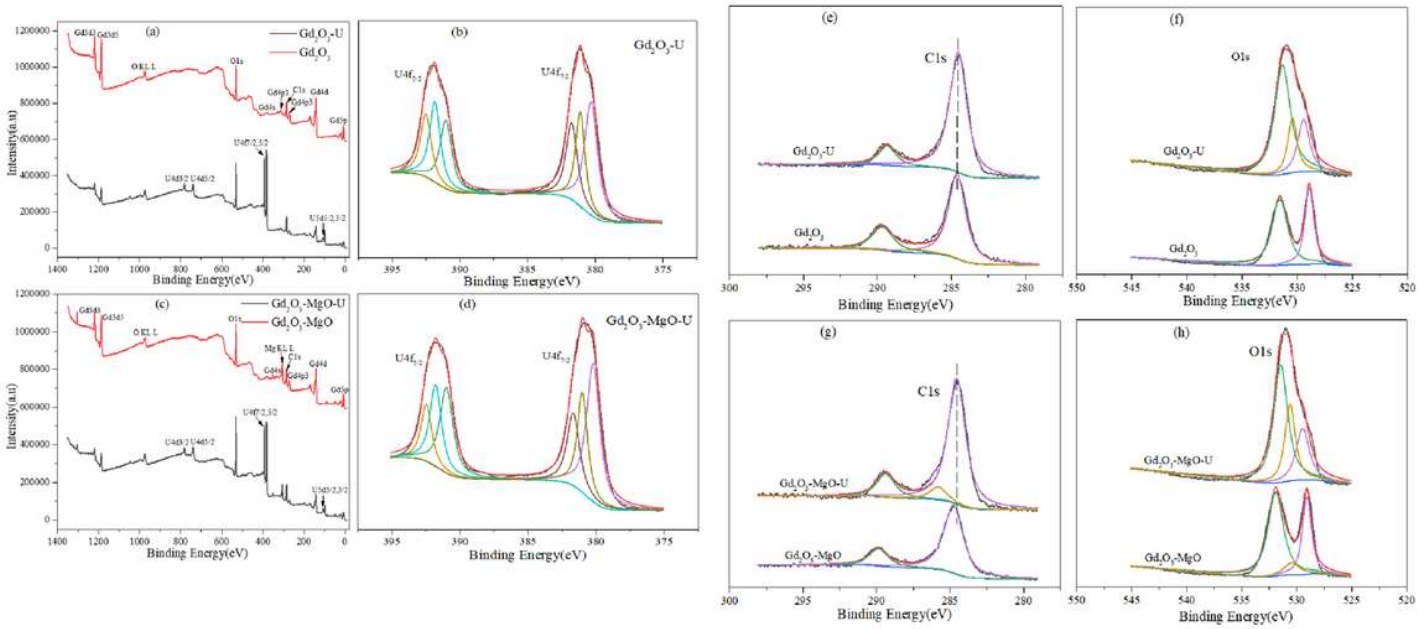


**Figure 9**

XPS spectra of Gd2O3 and Gd2O3-MgO.

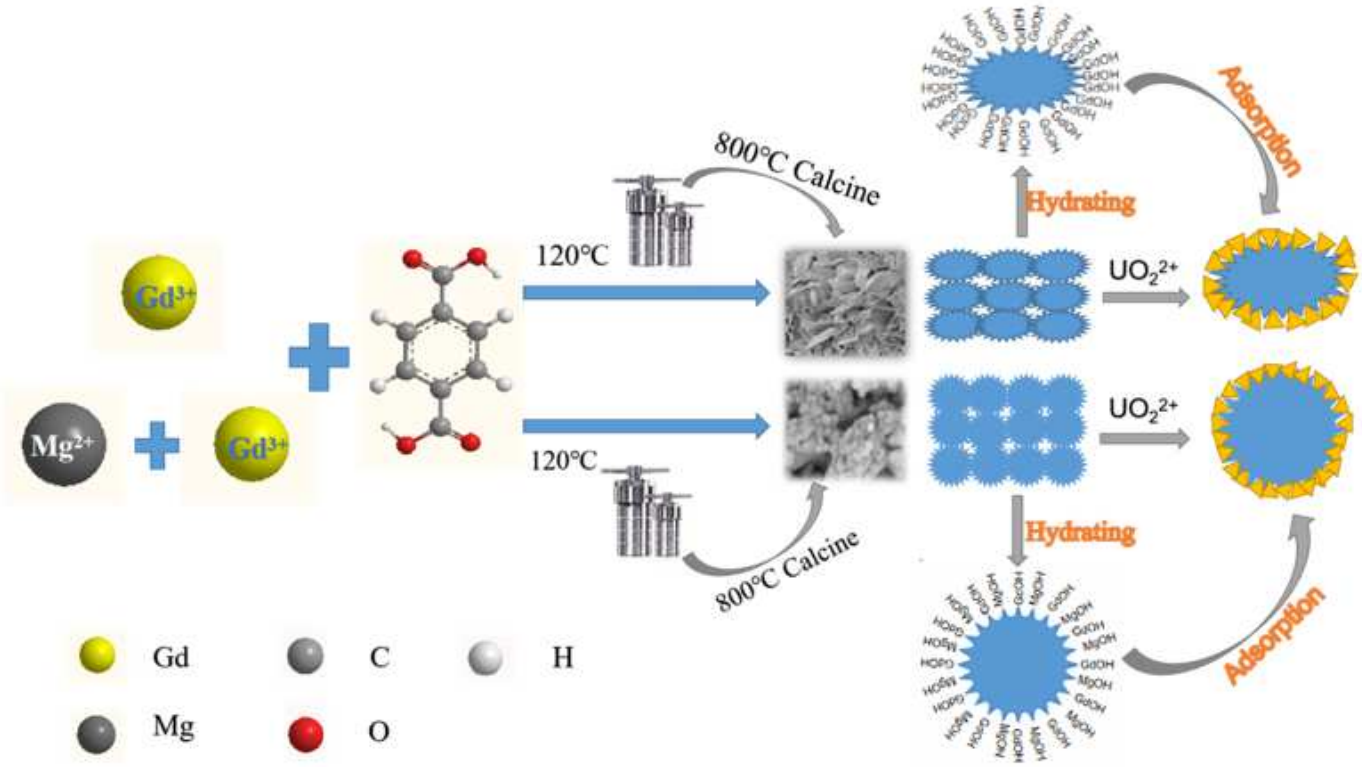


**Figure 10**

The surface adsorption of adsorbent for U(Ⅵ).